DEVELOPMENT OF MICRO-DIESEL INJECTOR NOZZLES VIA MEMS TECHNOLOGY AND EFFECTS ON SPRAY CHARACTERISTICS

Seunghyun Baik*, James P. Blanchard and Michael L. Corradini

Engine Research Center and Engineering Physics, University of Wisconsin, Madison, Wisconsin, USA

ABSTRACT

Micro-machined diesel injector nozzles have been designed, fabricated and used with commercially produced diesel injection systems in the study of spray dynamics. Such a system, properly designed, may improve spray behavior in DI diesel engines due to improved atomization and fuel-air mixing.

In this work, fourteen micro-planar orifice nozzles were fabricated using the MEMS (Micro-Electro-Mechanical-Systems) technique. Circular orifice diameters were varied from 40 to 260 microns and the number of orifices was varied from one to 169. Three plates with non-circular orifices were also fabricated to examine the effect of orifice shape on spray characteristics. These nozzles were then attached to commercial injectors and the associated injection systems were used for the spray experiments.

Given these novel injection systems, jet spray characteristics of micro-planar orifice nozzles were investigated experimentally using optical diagnostic techniques in a pressurized constant volume cylindrical chamber. Local drop sizes were measured by the laser diffraction technique, and average drop sizes of the whole sprays were measured by the light extinction

* Corresponding author : Address : 295 Roger Adams Laboratory, Box C-3, 600 South Mathews Avenue, Urbana, IL 61801, USA Tel: +1-217-333-5233 E-mail address: sbaik@scs.uiuc.edu

technique. Current test results show expected qualitative trends in spray kinematics and drop sizes, but quantitative magnitudes of the behavior are less dependent on orifice geometry than first anticipated. Droplet coalescence among adjacent sprays were apparent for the multiple orifice nozzles because all the orifices were aligned in the same direction with limited spacing. Non-planar configurations are under development and may show improved performance.

1 INTRODUCTION

MEMS (Micro-Electro-Mechanical-Systems) is a class of electro-mechanical systems that are fabricated to be very small; i.e., 1-100 micron sizes. These systems can have both electrical and mechanical components. MEMS originally used modified integrated circuit fabrication techniques and associated materials to create mechanical devices. Today, after years of research and development, there are many more fabrication techniques and material bases.

Silicon-based systems are in the process of altering conventional use of sensors, actuators and miniature mechanical devices [1]. It is a very versatile material but quite brittle under certain operating conditions. On the other hand, microstructures can be fabricated from metals via the LIGA process, which is based on deep-etch X-ray lithography, electroplating and molding [2-6]. The name “LIGA” comes from the German acronym, Lithographie, Galvanoformung and Abformung. The LIGA process was first developed at the Karlsruhe Nuclear Research Center for uranium enrichment purposes for the aerodynamic nozzle concept by Becker et al. [7]. Worldwide research activities on LIGA have been initiated more recently [4]. However, the LIGA process has not found a large number of industrial applications as yet and only a few realizations in micro-optics are expected to rapidly find industrial outlets. Nevertheless, the

fabrication of monolithic devices defined with a single deep X-ray lithographic step remains the most attractive applications of the LIGA process.

Based on the recent development of components for microfluid handling, there is a growing interest in research on these handling systems [8, 9] and the application of MEMS technology to the combustion and engine areas. Gardner et al. [10, 11] fabricated silicon micro-machined compound nozzles for SI engine fuel injectors. Micro-machined port fuel injectors were also fabricated by Hamid et al. [12] using laser drilling technology. Droplet coalescence among adjacent sprays was observed in the multiple–hole injectors which had up to a maximum of 1 mm spacing between orifices. Sufficient hole-to-hole separation was considered to be critical in avoiding droplet coalescence in future investigations. Kobori et al. [13] developed a micro-hole nozzle which has orifices with diameters as small as 60 microns using laser drilling technology. Combustion tests were carried out using a rapid compression-expansion machine that had a DI diesel type combustion chamber. There was a decrease in soot emission, whereas an increase in NO emission was observed.

A wider set of applications using the LIGA technology in fluidic devices are discussed by Madou [14]. Fluidic devices manufactured by the LIGA process have micron resolution, relatively high aspect ratio and flexibility in the choice of materials. The process reproducibility is also high. These characteristics give LIGA an advantage over silicon micromachining. Snyder [15] developed a Gas Efficient Liquid Atomization Device using the LIGA technology. One design of greater than 4000 holes at 7 microns produced average droplet sizes of less than 30 microns through gas assisted liquid film breakup.

In this work, micro-machined diesel injector nozzles have been developed using the LIGA technique and used with commercially produced diesel injection systems in the study of

spray dynamics. Such a system may have the capability to improve the spray characteristics in DI diesel engines due to the improved atomization and fuel-air mixing. The orifice diameter is an important variable for planar-orifice nozzles, and a number of drop size relations, showing decreasing drop sizes with decreasing orifice diameter, were summarized by Lefebvre [16]. The amount of fuel-air mixing was also shown to increase significantly with decreasing orifice diameter [17].

2 FABRICATION OF MICRO-PLANAR ORIFICE NOZZLES USING THE LIGA TECHNIQUE

Research at the University of Wisconsin in the LIGA area has been conducted for many years [18-20]. LIGA has many possible steps and the applied process sequence depends on the desired product. Detailed fabrication steps and nozzle designs are described in previous publications [21, 22].

Fourteen micro-planar orifice nozzles were fabricated using the LIGA technique, and Table 1 shows brief descriptions of each nozzle. The simple notations listed in the first column will be used to indicate each nozzle in this paper. The outer diameter of the nozzles is about 2.5 mm. The thickness is approximately 300 microns, which is the maximum thickness that could be manufactured with high throughput at the University of Wisconsin. The maximum achievable length over diameter ratio was about 10, which resulted in a minimum orifice size of 40 microns. All the orifices have orthogonal edges to the planar surface; i.e., zero injection angle. The nozzles are made of 78% nickel and 22% iron alloy; i.e., permalloy. Five plates that have a single orifice were fabricated to investigate the effect of orifice diameter on spray characteristics. The diameters were 40, 60, 80, 100 and 260 microns. 1x40 is shown in Fig. 1-a. As shown in

Fig. 1-b, 4x260 was fabricated to compare the performance to currently used diesel injector nozzles. The spacing between multiple orifices was varied in three other plates that each have five 40 micron orifices in order to investigate the effect of orifice spacing on interference among sprays. The spacings between orifices were 100, 150 and 200 microns. 5x40s150 is shown in Fig. 1-c. In addition, two plates that each have 41 orifices and 169 orifices, respectively, were fabricated. The number of 40 micron orifices was chosen so that each nozzle has the same mass flow area as another equivalent nozzle in which the orifice diameter is 260 microns. That is, 41x40 has the same flow area as that of 1x260, and 169x40 has the same flow area as that of 4x260. Figure 1-d shows 41x40, and Figure 2-a shows 169x40. Finally, three plates with non-circular orifices were also fabricated to examine the effect of orifice shape on spray characteristics. Figure 2-b shows 1xCross. Figure 2-c shows 1xTriangle, and Figure 2-d shows the enlarged picture of 4xTriangle. All three nozzles have the same flow area as that of 1x100.

3 EXPERIMENTAL SET-UP

Experiments were carried out for two different injection pressures, at room temperature and under quiescent gas conditions, in a pressurized constant volume cylindrical chamber (185 mm inner diameter and 185 mm long) equipped with two quartz windows with field of view 101 mm in diameter.

Measurements were performed on intermittent diesel sprays produced by a Bosch in-line fuel-injection pump. The pump was driven by a variable speed shunt DC motor through a semi-flexible coupling. A photo diode mounted on the pump shaft referenced the injection timing with respect to crank angle. California diesel fuel (ρ_f =841kg/m^3, ν=3.995cst) was used as a working fluid. A 7 micron filter was attached to the fuel line just before the Bosch in-line fuel-injection

pump to prevent plugging. A Bosch type rate of injection meter was used for all injection rate tracing [22, 23].

The injector used to demonstrate the micro-planar orifice nozzle operation for low injection pressures was an old LucasVarity injector. A new Bosch injector was used for high injection pressure experiments. Table 2 shows experimental conditions, and detailed descriptions will be discussed shortly. The very end of the commercial nozzle was cut, and the micro-planar orifice nozzle was attached to that end using a mechanical retainer. The design of the retainer is shown in Fig. 3.

Two pressure sensors were used for the low pressure experiments. As shown in Fig. 4, an absolute pressure sensor was installed anterior to the inlet of the LucasVarity injector using an adaptor. Therefore, the line pressure was detected by the absolute pressure sensor. The injector body was drilled, and a strain tube with an adaptor was also installed at the passage between the inlet of the injector and the nozzle sac. The fuel pressure was measured within the adaptor plate by the strain tube with strain gauges. The effect of the pressure sensors on the dynamics of the injector flow is expected to be minimal since the sensors do not obstruct the flow passage. A numerical study of the flow through a conventional diesel injector tip supports this hypothesis [24]. The work shows that almost all of the pressure drop through the tip occurs at the entrance of the orifice. Also, the acceleration between the needle and seat is very small compared to the acceleration through the orifice. For the high pressure experiments, only one absolute pressure sensor was installed anterior to the inlet of the Bosch injector.

Figure 5-a shows the low injection pressure profiles during the initial 5 ms for 1x40, 41x40 and 169x40. 1x40 and 169x40 respectively have the minimum and maximum flow areas. The injection pressures detected anterior to the inlet (i.e., line pressures) were almost invariant

for different nozzles. However, the injection pressures within the passage increased in oscillation about the inlet pressure as the nozzle flow area decreased. Nevertheless, the difference in averaged injection pressures was not significant, and the maximum injection pressures were determined to be about 20~25 MPa.

Figure 5-b shows the high injection pressure profiles during the initial 4 ms for 1x40 and 169x40. The nozzles with smaller total mass flow areas produced slightly higher maximum injection pressures. The maximum injection pressures were determined to be about 70~80 MPa.

In order to visually capture micro-nozzle sprays, a high speed digital camera, which was made by the Eastman Kodak Company (model 4540), was used at 4500 frames/second for recording the injection event. The images are digitized to 256 x 256 pixels with a gray scale of 256 levels. A video editor was also used to convert the images stored in the processor memory into video movies. A Questar QM-100 long distance microscopic lens was also used to acquire high magnification pictures. The light source was a pulsed copper-vapor laser (Oxford) rated up to 14 kHz repetition rate and 2 mJ per pulse with 20-60 ns pulse duration. Laser pulses were synchronized with the camera. A schematic of the optical set-up is given in Figure 6. Similar optical set-ups were also used by other investigators, and detailed descriptions are provided in previous publications [25, 26].

4. DROP SIZE MEASUREMENT TECHNIQUES

4.1 LASER DIFFRACTION TECHNIQUE

A laser diffraction based commercial system from Malvern/Insitec, the Spraytec ST218, was used to measure local drop sizes. The receiver focal length was 200 mm, and the corresponding detectable range of the volume median diameter was 5 to 250 microns. The range

of the size is based on the volume median diameter. Therefore, the actual range of the instrument is wider, in order to precisely measure droplets both above and below the volume median diameter [27]. The laser incorporated in the Spraytec was a diode laser and the laser beam diameter was 10 mm. Data were extracted with a sampling period of 0.4 ms. Thirty-one log scaled annular detector elements were used to measure the diffraction pattern. Each detector element was calibrated separately by Malvern/Insitec considering the variation in the responsivity of different detector elements.

The basic principles and limitations of the laser diffraction based particle sizing technique were summarized in the references [16, 27, 28], and a few limiting factors are discussed below. One of the assumptions for extending single scattering relations to poly-dispersed particles is the absence of multiple scattering. Light obscuration can be used as a major indicator of the extent to which the measurements are being affected by multiple scattering. Malvern/Insitec developed a multiple scattering correction algorithm that can measure particle distributions with light transmission values as low as 2 percent [27]. The largest mass flow area nozzle (169x40) produced the minimum averaged transmission value over injection durations, at high injection pressures, and it was about 15 percent.

When taking measurements in sprays, it is necessary to limit the maximum distance between the spray and the receiving optics. Exceeding this distance results in vignetting of the signal on the outer rings. For the experiments in this work, the spray was placed within 1.5 times the focal length from the receiving optics to avoid vignetting, which was recommended by Malvern/Insitec.

4.2 LIGHT EXTINCTION TECHNIQUE

The light extinction technique was used in order to measure the average drop sizes of the whole spray. The basic theory relates the attenuation of a collimated monochromatic laser that passes through a poly-disperse droplet field to the average droplet size of the whole spray. The final formulation for the Sauter Mean Diameter (SMD) is given below, and the detailed derivation is given in the references [25, 26, 29, 30].

$$D_{32} = \frac{\sum N_i D_i^3}{\sum N_i D_i^2} = \frac{3M_f \overline{RQ_{ext}}}{2a_p \rho_f \sum_{j=1}^{P} (-\ln \tau_j)} \tag{1}$$

M_f is the total fuel mass in the instantaneous spray image, ρ_f is the density of fuel, a_p is the cross sectional area of each pixel, τ_j is the transmittance of the j^{th} optical path inside the spray and $\overline{RQ_{ext}}$ is the averaged corrected extinction coefficient.

Kamimoto et al. [30] used glass beads in ethyl alchol as test particles in order to verify the light extinction technique. The SMD measured by the light extinction technique and the SMD measured by photographs were compared, and the error was about 10 %.

El-beshbeeshy [29] and Goney [25] used similar experimental set-ups as was used for the experiments in this paper and carried out error analyses based on Eq. (2). The maximum error was estimated by analyzing two input variables, mass and transmittance, independently.

$$\left|\frac{\Delta D_{32}}{D_{32}}\right| = \left|\frac{\partial D_{32}\Delta M_f}{\partial M_f D_{32}}\right| + \left|\frac{\partial D_{32}\Delta \tau_j}{\partial \tau_j D_{32}}\right| = \left|\frac{\Delta M_f}{M_f}\right| + \left|\frac{\sum_{j=1}^{p} \frac{\Delta \tau_j}{\tau_j}}{\sum_{j=1}^{p} -\ln \tau_j}\right| \tag{2}$$

El-beshbeeshy [29] evaluated the term $\left|\frac{\Delta M_f}{M_f}\right|$ from the resolution of the electronic scale. This resulted in a maximum error of ± 1 %. However, shot to shot variation of the injected mass

and of the rate of injection was not considered in the analysis of El-beshbeeshy. Shot-to-shot variation could not be measured because the cumulative mass from thousands of injections was divided by the number of injections to obtain the averaged mass of a single injection using a Bosch type rate of injection meter [22, 23]. Also, possible error in estimating the precise starting time of an injection could lead to mass error, as will be discussed later. The mass error at the early stages of injection could be large because the denominator in the term $\left|\frac{\Delta M_f}{M_f}\right|$ is very small. The light extinction technique resulted in large variation in SMD at the early stages of injection for some cases in this work and others [31], due to possible mass error. The transient SMD at the early stages of injection was excluded from the calculation of the averaged SMD of micro-nozzles.

El-beshbeeshy [29] evaluated the transmittance error term $\left|\frac{\sum_{j=1}^{p}\frac{\Delta\tau_j}{\tau_j}}{\sum_{j=1}^{p}-\ln\tau_j}\right|$ as resulting from the calibration using a finite number of optical density filters. Twelve reflective optical density filters ranging from 0.1 to 1 were used for the experiments of El-beshbeeshy, and transmittances other than the 12 values were calibrated using a linear regression line. The error from the linear regression line resulted in a maximum error of ± 7 %. Goney [25] also concluded that the maximum error was in the transmittance calibration part from the above analysis, and concentrated on the improvement of the calibration by changing optical density filters from the reflective type to the absorptive type. Reflective optical density filters produced interference patterned images due to the reflections at the surfaces of the reflective filters. Thirteen values from absorptive neutral density filters were used for this study.

5 EXPERIMENTAL RESULTS

Fourteen micro-planar orifice nozzles were divided into four groups in order to systematically compare the spray characteristics, such as spray tip penetrations, spray cone angles, drop sizes and spray images; i.e., single orifice nozzles, multiple orifice nozzles, nozzles with different orifice shapes and shower head nozzles.

5.1 SINGLE ORIFICE NOZZLES

Five plates that have a single orifice were fabricated to investigate the effect of orifice diameter on spray characteristics. The diameters were 40, 60, 80, 100 and 260 microns. The spray breakup regimes are shown in Fig. 7. The data moved from the atomization regime to the second wind-induced regime near the borderline as the orifice diameter decreased. A decrease in the orifice diameter resulted in a decrease in the Reynolds number. A large decrease in the Reynolds number suggests a decrease in turbulence, which has a negative effect on atomization. However, the smaller orifice nozzles produced smaller drop sizes, as will be discussed shortly.

Spray characteristics of five injection events were measured and analyzed for each nozzle at low and at high injection pressures. For reasons of clarity, only polynomial regression curve fits of the spray tip penetration lengths are shown in Fig. 8. Standard deviations (SD) in millimeters are also given next to the nozzle legends. Nitrogen gas was used to pressurize the chamber for the low injection pressure experiments, and the gas density inside the chamber was 11.85 kg/m^3. For the high injection pressure experiments, argon gas was used to pressurize the chamber, and the gas density inside the chamber was 18.9 kg/m^3. Due to the larger molecular weight of argon, a larger density could be achieved with a lower pressure compared to the

nitrogen gas. The increase in density was needed to prevent the spray tip from reaching the end of the window too quickly. The precise starting time of the injection could not be measured more accurately than the temporal resolution of the high speed camera, and the temporal resolution used in this study was about 0.22 ms. Therefore, the polynomial regression curve fit was used to determine the start of injection as an approximation. The offset on the time axis was shifted to zero, and the adjusted time was used for the data analysis in this work. For the low pressure experiments, the spray tip penetrating speeds, which can be inferred from the slopes of the data, decreased significantly as the orifice diameter decreased from 260 microns to 40 microns as shown in Fig. 8-a. The spray tip penetration data were compared to the penetration relation proposed by Arai et. al [32].

$$0<t<t_b,\ S=0.39\sqrt{\frac{2\Delta P}{\rho_l}}\,t \qquad t_b=28.65\,\frac{\rho_l D}{\sqrt{\rho_a \Delta P}} \qquad t>t_b,\ S=2.95\left(\frac{\Delta P}{\rho_a}\right)^{0.25}\sqrt{Dt} \qquad (3)$$

t_b is the breakup time, ΔP is the pressure difference across the orifice, ρ_l is the fuel density, ρ_a is the air density and D is the orifice diameter.

The averaged injection pressure over 1~3 ms was used for the penetration relation because the relation was originally developed for a constant injection pressure profile during the injection, i.e., a top hat profile. The penetration relation underpredicted the data at the low chamber gas density of 11.9 kg/m^3. Naber and Siebers [33] also noted that Eq. (3) tends to underpredict penetration at low gas densities.

Similar penetration trends could be observed at high injection pressures as shown in Fig. 8-b. There was a reasonable agreement between the data and the penetration relation at the high chamber gas density of 18.9 kg/m^3. The dependence of the penetration lengths on the orifice diameter seemed to be reasonably predicted by the relation.

Figure 9 shows ensemble averaged spray cone angles and standard deviations measured at 20 mm away from the nozzle tip. Spray cone angles were directly measured from the enlarged spray pictures. Both high and low pressure data are presented. After an initial transient period, when the measured spray angle varied with time, a quasi-steady period was reached. The transient data at the early stages of injection were excluded from the calculation of the averaged spray cone angles. The spray cone angles decreased as the orifice diameter decreased. The spray cone angles at high injection pressures were larger than those at low injection pressures.

Figure 10 shows ensemble averaged SMD over injection durations measured using Malvern. Standard deviations in micrometers are shown next to the symbols. Drop sizes at low injection pressures were measured at the middle of the spray at 25~35 mm away from the nozzle tip and 15~25 mm away from the nozzle tip. Drop sizes at high injection pressures were measured at the middle of the spray at 30~40 mm away from the nozzle tip and 20~30 mm away from the nozzle tip. The laser beam diameter was 10 mm and the corresponding measurement area was 79 mm^2. The SMD measured downstream was generally larger than that upstream, possibly due to droplet coalescence. The SMD decreased as the orifice diameter decreased. The SMD at high injection pressures was smaller than that at low injection pressures.

Figure 11 shows ensemble averaged SMD and standard deviations at high injection pressures measured by the two different techniques. The average drop sizes of the whole sprays were measured by the light extinction technique. The two different measurement techniques produced qualitatively similar trends as the diameter of orifices changed. The quantitative differences may originate from the different relative Malvern measurement locations compared to the tip of sprays, resulting from the different spray tip penetrating speeds. The spray image of 1x40 at a time 4 ms after start of injection and the spray image of 1x260 at a time 1.5 ms after

start of injection, measured at high injection pressures, are shown in Fig. 12. Figure 12-a was taken at the end of the injection event to show the largest image. Figure 12-b was taken right before the spray tip reached the end of the window to avoid cropping the image. The absorptive neutral density filters for the light extinction method are shown at the sides. The Malvern measurement locations are shown at the center of the spray. The smaller mass flow area nozzle (1x40) produced slower spray tip penetrating speeds, and the drop sizes near the tip were measured using Malvern. Drop sizes measured downstream were larger than those upstream from the Malvern results. Therefore, the drop sizes near the tip may be larger than the average drop sizes of the whole spray. In contrast, the drop sizes relatively upstream were measured using Malvern for the larger mass flow area nozzle (1x260). The drop sizes upstream may be smaller than the average drop sizes of the whole spray, due to the increased drop sizes further downstream.

5.2 MULTIPLE ORIFICE NOZZLES

The number of 40 micron diameter orifices was varied from one to 169. The polynomial regression curve fits and standard deviations of spray tip penetration lengths of multiple orifice nozzles at high and at low injection pressures are shown in Fig. 13. The spray tip penetrating speeds increased as the number of orifices increased. However, there was no noticeable difference in penetrating speeds among the five 40 micron orifice nozzles with different spacings between orifices.

The spray images of 1x40, 5x40s200, 41x40 and 169x40 at high injection pressures are shown in Fig. 14. Background images were subtracted for reasons of clarity, and all the images

have the same magnification. The spray from a large number of small orifices resembles that from a single large orifice.

The ensemble averaged spray cone angles and standard deviations measured at 20 mm away from the nozzle tip are shown in Fig. 15. The spray cone angles increased as the number of orifices increased. Higher injection pressures produced larger spray cone angles. However, there was no noticeable difference in spray cone angles among the five 40 micron orifice nozzles with different spacings between orifices.

The ensemble averaged drop sizes and standard deviations measured using Malvern are shown in Fig. 16. Drop sizes at low injection pressures were measured at the middle of the spray at 25~35 mm away from the nozzle tip and 15~25 mm away from the nozzle tip. Drop sizes at high injection pressures were measured at the middle of the spray at 30~40 mm away from the nozzle tip and 20~30 mm away from the nozzle tip. The SMD measured downstream was larger than that upstream, possibly due to droplet coalescence. Higher injection pressures produced smaller SMD. The SMD increased as the number of orifices increased. However, there was no noticeable difference in SMD among the five 40 micron orifice nozzles with different spacings between orifices. All the orifices in our nozzles are aligned in the same direction; i. e., zero injection angle. The maximum spacing that can be made at the end of the diesel injector nozzle tip is about 1 mm. However, the sprays are in centimeter scales. Therefore, the interference among adjacent sprays could not be avoided in the multiple orifice nozzles for diesel injectors, which probably led to droplet coalescence. The different spacings between orifices within the range of our designs do not seem to affect spray characteristics much.

Figure 17 shows ensemble averaged drop sizes and standard deviations measured at high injection pressures by the two different techniques. Similar to the single orifice nozzles, the

average drop sizes of the whole sprays of the smaller mass flow area nozzles were smaller than the local drop sizes measured using Malvern. For the larger mass flow area nozzles, 41x40 and 169x40, the average drop sizes were larger than the local drop sizes.

5.3 DIFFERENT ORIFICE SHAPE NOZZLES

Three plates with non-circular orifices were fabricated to examine the effect of orifice shape on spray characteristics. Schwesinger and Bohmann [34] investigated liquid jets injected from triangular shaped micro-channels. The liquid jet deflected from the axis of injection, and the deflection direction depended on the angle of the triangle. However, the deflection decreased as the liquid injection velocity increased. It is of interest, therefore, to investigate spray characteristics of different orifice shape nozzles including triangular geometry. All the non-circular orifice nozzles have the same flow area as that of 1x100. The spray penetration lengths at low and at high injection pressures are shown in Fig. 18. The spray cone angles are shown in Fig. 19. There was no noticeable difference in spray tip penetrating speeds, spray cone angles and spray images. There were similar trends for both high and low injection pressure data, and deflections could not be observed with the investigated injection pressures.

The drop sizes measured using Malvern are shown in Fig. 20. All the nozzles produced similar SMD except for 4xTriangle at low injection pressures. This will be discussed further later. The different orifice shapes within the range of our designs do not seem to affect the spray characteristics much, as long as they are single orifice nozzles.

Figure 21 shows the drop sizes measured at high injection pressures by the two different techniques. According to the light extinction results, the average drop sizes of 4xTriangle were larger than those of 1xTriangle. This will also be discussed further later. The average drop sizes

of 1x100 were slightly larger than those of other single non-circular orifice nozzles. The reason for the difference is not clearly identified, but there is not much difference in values.

5.4 SHOWER HEAD NOZZLES

41x40 has the same flow area as that of 1x260, and 169x40 has the same flow area as that of 4x260. The spray tip penetration lengths at low and at high injection pressures are shown in Fig. 22, and the spray cone angles are shown in Fig. 23. The spray tip penetrating speeds and cone angles of 41x40 were similar to those of 1x260. The spray tip penetrating speeds and cone angles of 169x40 were similar to those of 4x260. Nozzles with the same flow areas produced similar penetrating speeds, cone angles and spray images regardless of single, multiple or shower head designs, at both high and low injection pressures.

The drop sizes measured using Malvern are shown in Fig. 24. At low injection pressures, the SMD of 41x40 was larger than that of 1x260 at the two central measurement locations. The multiple orifice nozzle produced larger SMD than that of the single orifice nozzle with the same mass flow area. This suggests that a large number of droplet coalescence may be occurring at the measurement locations. On the other hand, at high injection pressures, 41x40 produced SMD similar to that of 1x260. This will be discussed further later.

At low injection pressures, the SMD of 169x40 was smaller than that of 4x260. A nozzle with a large number of small orifices produced smaller SMD than a nozzle with a few large orifices, having identical mass flow area. At high injection pressures, nozzles with the same flow area produced similar SMD.

Drop sizes measured by the two different techniques are shown in Fig. 25. The trends in the average drop sizes of the whole sprays at high injection pressures were similar to those in local drop sizes at low injection pressures. This will also be discussed further shortly.

5. 5 SUGGESTED DROPLET COLLISION DYNAMICS

Schematic diagrams of sprays from a single orifice nozzle and a multiple orifice nozzle are shown in Fig. 26. From a macroscopic view point, the spray from the single orifice nozzle has an axial velocity component and radial diverging velocity components. Of course, there will be a large number of droplet collisions inside the spray at microscopic scales. However, the diverging velocity components of adjacent sprays from the multiple orifice nozzle collide with each other even at macroscopic scales. Sprays from the multiple orifice nozzle are more likely to undergo droplet collisions due to the interference among adjacent sprays.

The drop sizes of 1x260 and 41x40, with the same mass flow area, are shown again in Fig. 27. At low injection pressures, the drop sizes of 41x40 were larger than those of 1x260 at the two central Malvern measurement locations, possibly due to droplet coalescence. At high injection pressures, initial fuel injection velocities will be higher than those at low injection pressures due to greater pressure differences. The higher initial injection velocities will lead to higher relative collision velocities when droplet collisions occur at the two central Malvern measurement locations. The higher relative collision velocities will lead to less droplet coalescence and more shattering [35]. This may be the reason for the similar drop sizes at the two central Malvern measurement locations at high injection pressures.

In any case, the droplets will keep on colliding at the reduced velocities further downstream, even at high injection pressures. This will lead to more droplet coalescence further

downstream, resulting in larger average drop sizes of the whole sprays of the multiple orifice nozzle compared to those of the single orifice nozzle.

The drop sizes of 1xTriangle and 4xTriangle are shown again in Fig. 28. Similar trends in drop sizes could be observed for these nozzles.

5.6 MICROSCOPIC VIEWS AT NOZZLE EXITS

A microscopic lens was used in order to visualize near tip spray images. A video editor was also used to convert the images stored in the processor memory into video movies. Spray images of selected micro-nozzles with representative characteristics are given in this section. The depth of the focal plane was smaller than the size of micro-nozzles. Therefore, some sprays of the multiple orifice nozzles were out of the focal plane and could not be simultaneously focused. The maximum length shown in the images is about 1.5 mm, and the resolution is about 1.5mm / 256 pixels, i.e., 5.9 μm / pixel. All the sprays were parallel to the high speed digital camera.

Figure 29 shows the spray images of 1x40 at low and at high injection pressures. A mechanical retainer is shown at the top of each image, and the actual nozzle exit is about 1 mm above. The spray at high injection pressures seems to have better atomization.

Figure 30 shows the spray images of 1x260. The central region of the spray was somewhat transparent at low injection pressures. The edges seem to have better atomization. However, the transparent core could not be observed at high injection pressures.

Figure 31 shows the spray images of 5x40s200. Individual spray columns could not be observed at high injection pressures.

Figure 32 shows the spray images of 41x40. For the low injection pressure experiments, individual spray columns could not be observed except at the end of the injection event, when

the injection pressure is low. Individual spray columns could not be observed at all at high injection pressures.

Figure 33 shows the spray images of 169x40. Individual spray columns could not be observed at all at high and at low injection pressures.

6 CONCLUSION

Micro-machined diesel injector nozzles have been designed, fabricated and used with commercially produced diesel injection systems. The major focus of this work was to demonstrate that the MEMS (Micro-Electro-Mechanical-Systems) technique can be used to fabricate nozzle tips of arbitrary shapes and sizes for real diesel injector nozzles.

In this work, fourteen micro-planar orifice nozzles were fabricated using the LIGA technique (deep X-ray lithography and electroplating technology). The circular orifice diameters were varied from 40 to 260 microns and the number of orifices was varied from one to 169. Three plates with non-circular orifices were also fabricated to examine the effect of orifice shape on spray characteristics. These nozzles were then attached to commercial diesel injectors and the associated injection systems were used for the spray experiments.

Given these novel injection systems, jet spray characteristics of micro-machined planar orifice nozzles were investigated experimentally at two different injection pressures (around 25 MPa and 80 MPa) using optical diagnostic techniques, at room temperature and under quiescent gas conditions, in a pressurized constant volume cylindrical chamber at prototypic densities. Local drop sizes were measured by the laser diffraction technique, and the average drop sizes of the whole sprays were measured by the light extinction technique. Current test results show expected qualitative trends in spray kinematics and drop size, but the quantitative magnitudes of

the behavior are less dependent on geometry than first anticipated. The following observations were obtained within the range of our designs :

- The spray tip penetrating speeds and cone angles primarily depended on the total mass flow area regardless of single or multi-hole or different geometry. The spray tip penetrating speeds and cone angles decreased as the total mass flow area decreased.
- The SMD decreased as the diameter of orifices decreased in a non-linear fashion.
- The SMD increased as the number of orifices increased, possibly due to agglomeration effects.
- *The different geometry of single orifice nozzles did not affect the SMD significantly.*
- Higher injection pressures produced faster spray tip penetrating speeds, larger cone angles and smaller SMD.

According to the experimental results, droplet coalescence among adjacent sprays were apparent for the multiple orifice nozzles. Droplet coalescence could not be avoided because all the orifices in the micro-planar orifice nozzles were aligned in the same direction with limited spacing (maximum 200 microns), i.e., zero injection angle. In light of these facts, a new set of non-planar micro-nozzles are under development and may show improved performance.

ACKNOWLEDGEMENTS

The authors would like to acknowledge the financial support of the Army Research Office and S.C. Johnson Wax and the technical assistance provided by the Wisconsin Center for Applied Micromechanics.

REFERENCES

1. K. E. Peterson, Silicon as a Mechanical Material, Proc. IEEE, vol. 70, No.5, pp.420-457, 1982
2. H. Guckel, T. Christenson, K. Skrobis, Metal Micromechanisms via Deep X-Ray Lithography, Electroplating and Assembly, J.Micomech. Microeng. 2, pp.225-228, 1992
3. S. Ballandras et al., Deep Etch X-Ray Lithography using Silicon-Gold Masks Fabricated by Deep Etch UV Lithography and Electroforming, J. Micromech. Microeng. 5, pp.203-208, 1995
4. A. Rogner, J. Eicher, D. Munchmeyer, R-P. Peters, J. Mohr, The LIGA Technique-What are the New Opportunities, J.Micromech. Microeng. 2, pp. 133-140, 1992
5. H. Guckel, K. Skrobis, T. Christensen, J. Klein, Micromechanics for Actuators via Deep X-Ray Lithography, Proc. SPIE's 1994 Symposium on Microlithography, pp. 39-47, San Jose, CA, March, 1994
6. H. Guckel, Deep X-Ray Lithography for Micromechanics and Precision Engineering, Synchrotron Radiation Instrumentation (Invited), Advanced Photon Source, Argonne, IL, October, 1995
7. E. W. Becker, W. Bier, K. Ehrfeld, K. Schubert, R. Schutte, D. Seidel, Uranium Enrichment by the Separation Nozzle Process, Naturwissenschaften 63, pp. 407-411, 1976
8. P. Gravesen, J. Branebjerg, O. Jensen, Microfluidics a Review, J. Micromech. Microeng. 3, pp. 168-182, 1993
9. W. Schomburg, J. Vollmer, B. Bustgens, J. Fahrenberg, H. Hein, W. Menz, Microfluidic Components in LIGA Technique, J. Micromech. Microengr. 4, pp.186-191, 1994
10. R. Gardner, W. Horn, M. Rhoades, M. Wells, S. Yockey, Silicon Mocromachined Compound Nozzle, United States Patent, Patent Number 4828184, May 9, 1989
11. R. Gardner, J. Giachino, W. Hora, M. Rhoades, M. Wells, S. Yockey, Fuel Injector with Silicon

Nozzle, United States Patent, Patent Number 4907748, March 13, 1990

12. M. Hamid, H. Kim, K. Im, M. Lai, H. Nuglisch, J. Dressler, Effect of Pressure Modulation on Micro-Machined Port Fuel Injector Performance, Eighth International Conference on Liquid Atomization & Spray Systems, Pasadena, CA, pp. 546~551, 2000
13. S. Kobori, T. Kamimoto, H. Kosaka, Ignition, Combustion and Emissions in a DI Diesel Engine Equipped with a Micro-Hole Nozzle, SAE 960321, 1996
14. M. Madou, 'Fundamentals of Microfabrication', CRC Press, 1997
15. H. Snyder, Efficient Liquid Atomization using Gas Flows and Novel Micro-Machining Techniques, Ph.D. Thesis, University of Wisconsin, Madison, WI, 1997
16. A. H. Lefebvre, Atomization and Sprays, Taylor & Francis, 1989
17. D. Siebers, B. Higgins, Flame Lift-Off on Direct-Injection Diesel Sprays Under Quiescent Conditions, SAE 2001-01-0530, 2001
18. J. Klein, Preliminary Results of a Micro-Induction Motor, PhD Thesis, University of Wisconsin, Madison, WI, 1998
19. B. Chaudhuri, Reduction of Bounce in the Closure of Contacts through Damping in a Magnetic Field, PhD Thesis, University of Wisconsin, Madison, WI, 2000.
20. K. Fischer, A LIGA Fabricated Latching, Bistable Magnetic Micro Actuator for Optical Fiber Switching and Other Applications, PhD Thesis, University of Wisconsin, Madison, WI, 2000
21. S. Baik, K. Goney, S. Kang, J. Murphy, J. Blanchard, M. Corradini, Development of Micro-Diesel Injector Nozzles via MEMS Technology and Initial Results for Diesel Sprays, SAE 1999-01-3645, 1999
22. S. Baik, Development of Micro-Diesel Injector Nozzles via MEMS Technology and Effects on Spray Characteristics, PhD Thesis, University of Wisconsin, Madison, WI, 2001

23. G. Bower, D.E. Foster, A Comparison of the Bosch and Zuech Rate of Injection Meters, SAE 910724, 1991
24. D. P. Schmidt, C. J. Rutland, M. L. Corradini, A Numerical Study of Cavitating Flow through Various Nozzle Shapes, SAE 971597, 1997
25. K. Goney, Investigation of Internal Nozzle Multiphase Flow and Its Effects on Diesel Sprays, Ph. D. Thesis, University of Wisconsin, Madison, WI, 2000
26. M. El-beshbeeshy, J. Hodges, M. Corradini, Image Analysis of Diesel Sprays, SAE 921628, 1992
27. EPCS Technical Specification Revision 21.1.98.2, Malvern Instruments
28. S. Parrish, Spray Characterization in a Motored Direct-Injection Spark-Ignited Engine, Ph.D. Thesis, University of Wisconsin, Madison, WI, 1997
29. M. El-beshbeeshy, Image Analysis of Sprays by Light Extinction Technique, Ph. D. Thesis, University of Wisconsin, Madison, WI, 1992
30. T. Kamimoto, H. Yokota, H. Kobayashi, A New Technique for the Measurement of Sauter Mean Diameter of Droplets in Unsteady Dense Sprays, SAE 890315, 1989
31. W. Chang, P. Farrell, Comparison of Spray Characteristics for Two GDI Fuel Injectors, ASME Internal Combustion Engine Division, 2000 Fall Technical Conference, September, 2000
32. M. Arai, M. Tabata, H. Hiroyasu, M. Shimizu, Disintegrating Process and Spray Characterization of Fuel Jet Injected by a Diesel Nozzle, SAE 840275, 1984
33. J. Naber, D. Siebers, Effects on Gas Density and Vaporization on Penetration and Dispersion of Diesel Sprays, SAE 960034, 1996
34. N. Schwesinger, W. Bohmann, The Behavior of Liquid Jets Escaping Microchannels, J. Micromech. Microengr. 3, pp.210-213, 1993

35. N. Ashgriz, J.Y. Poo, Coalescence and Separation in Binary Collisions of Liquid Drops, J. Fluid Mech., vol. 221, pp. 183-204, 1990

Notation	Description
1x40	single 40 micron circular orifice nozzle
1x60	single 60 micron circular orifice nozzle
1x80	single 80 micron circular orifice nozzle
1x100	single 100 micron circular orifice nozzle
1x260	single 260 micron circular orifice nozzle
4x260	four 260 micron circular orifice nozzle
5x40s100	five 40 micron circular orifice nozzle with 100 micron spacing between orifices
5x40s150	five 40 micron circular orifice nozzle with 150 micron spacing between orifices
5x40s200	five 40 micron circular orifice nozzle with 200 micron spacing between orifices
41x40	41 circular orifice nozzle with an orifice diameter of 40 microns
169x40	169 circular orifice nozzle with an orifice diameter of 40 microns
1xCross	single cross shaped orifice nozzle
1xTriangle	single triangular shaped orifice nozzle
4xTriangle	four triangular shaped orifice nozzle

Table 1. Micro-planar orifice nozzles

Experimental conditions	Maximum injection pressures	Spray chamber density
High pressure experiments	20 ~ 25 MPa	11.85 kg/m^3 (nitrogen gas)
Low pressure experiments	70 ~ 80 MPa	18.9 kg/m^3 (argon gas)

Table 2. Experimental conditions

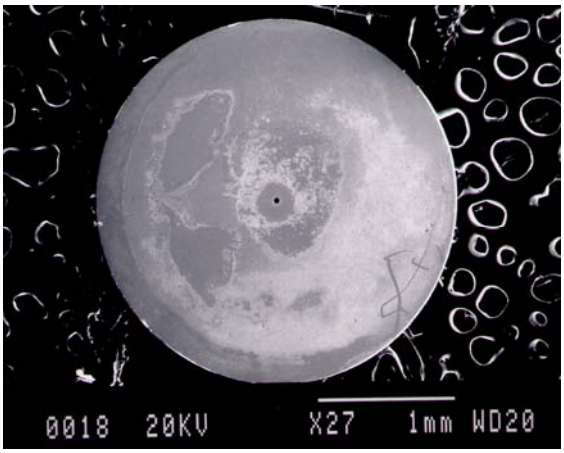

(a)

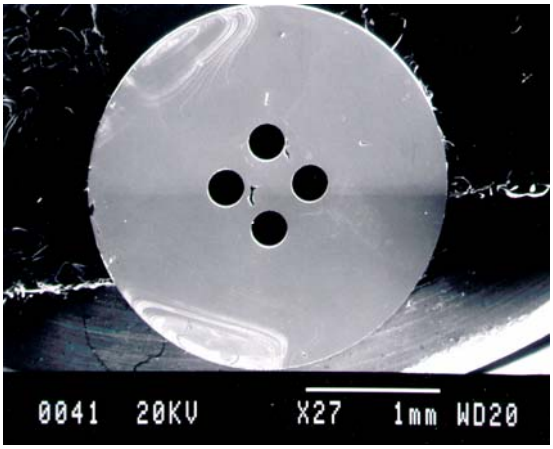

(b)

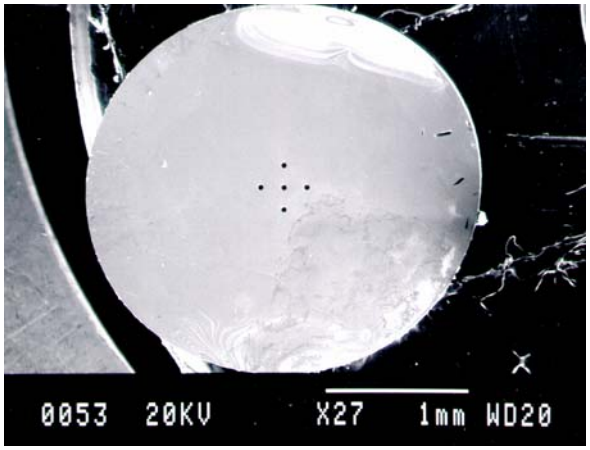

(c)

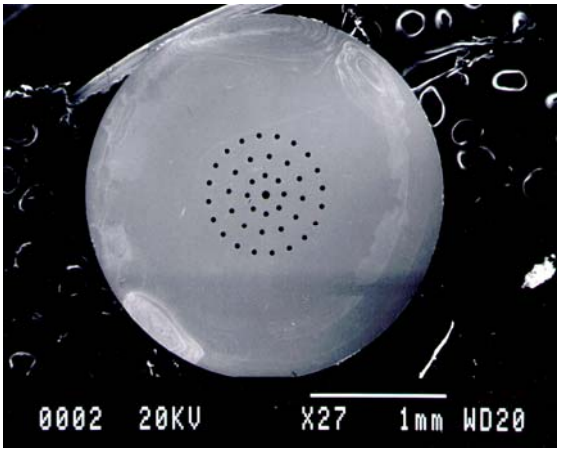

(d)

Figure 1 Micro-planar orifice nozzles - I (a) 1x40 (b) 4x260 (c) 5x40s150 (d) 41x40

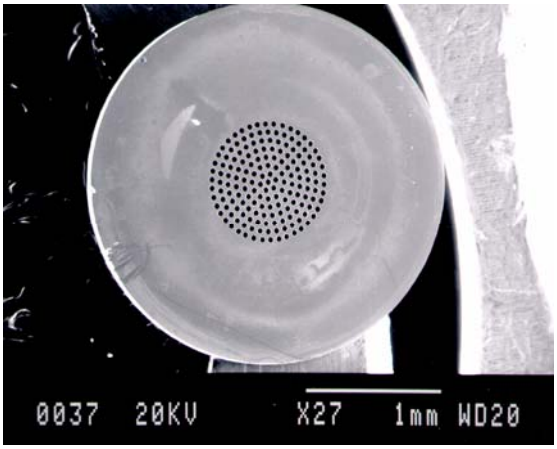

(a)

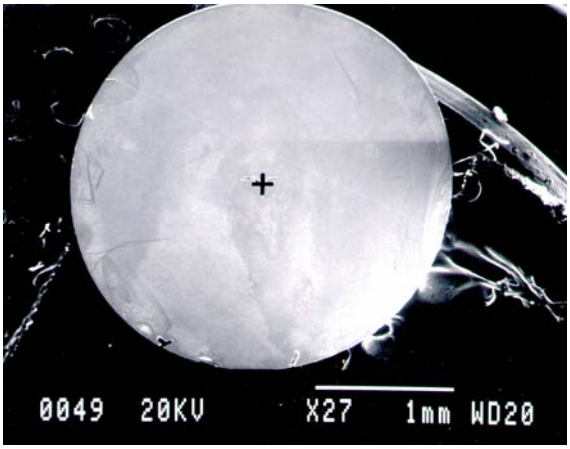

(b)

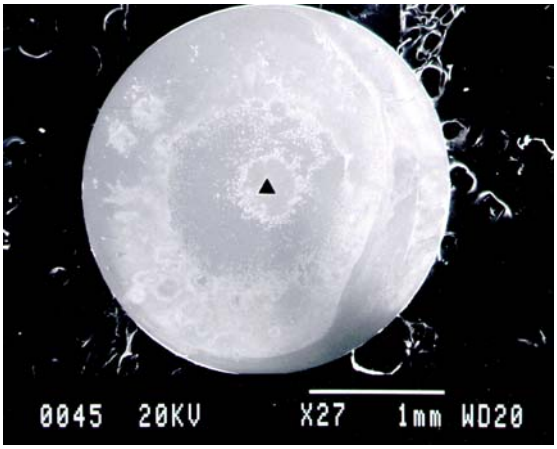

(c)

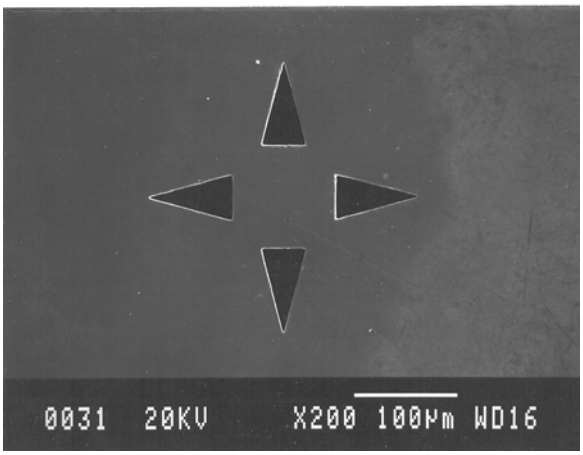

(d)

Figure 2 Micro-planar orifice nozzles - II (a) 169x40 (b) 1xCross (c) 1xTriangle (d) 4xTriangle

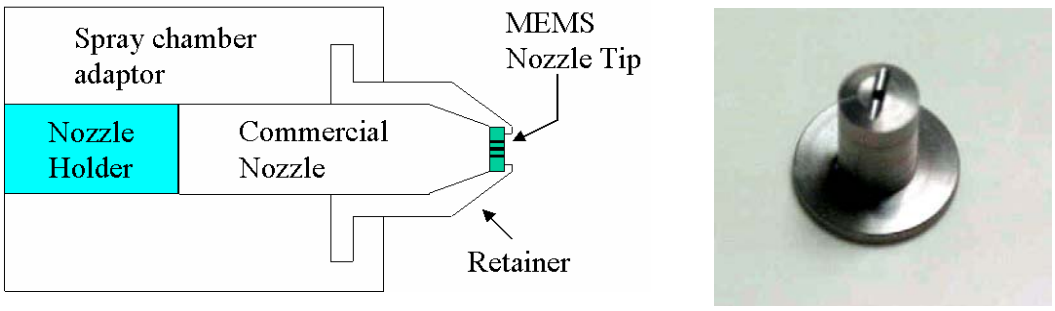

Figure 3 The mechanical retainer design

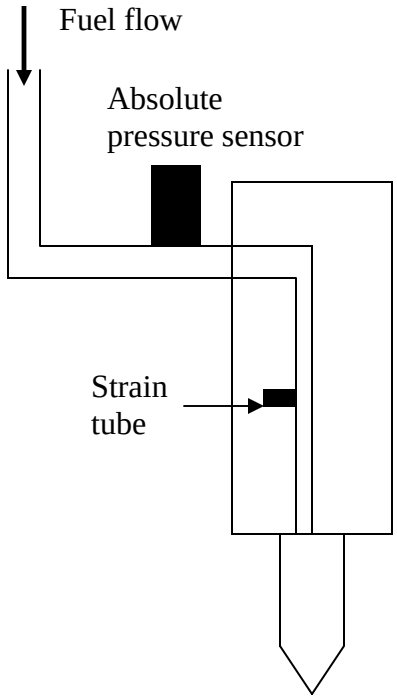

Figure 4 Injection pressure sensor locations

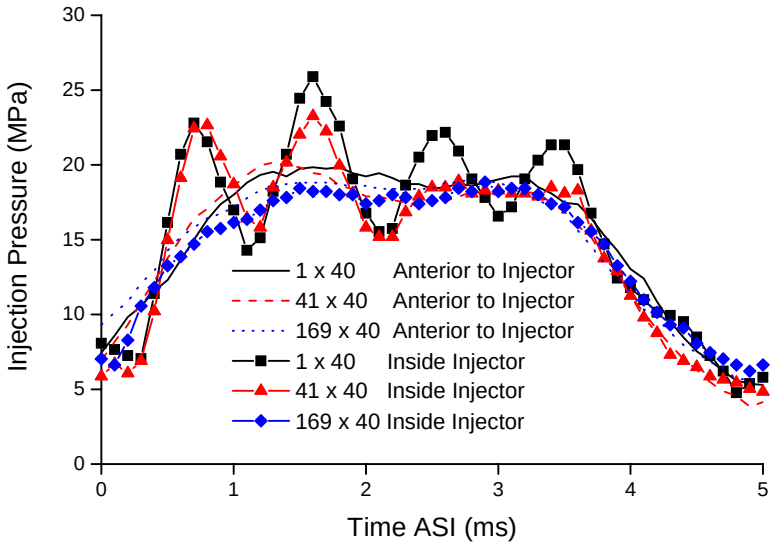

(a)

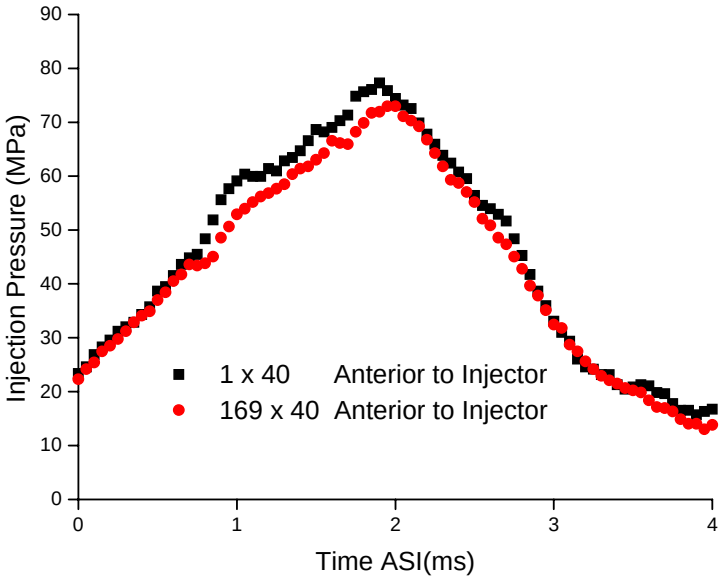

(b)

Figure 5 Injection pressure profiles (a) low injection pressures (b) high injection pressures

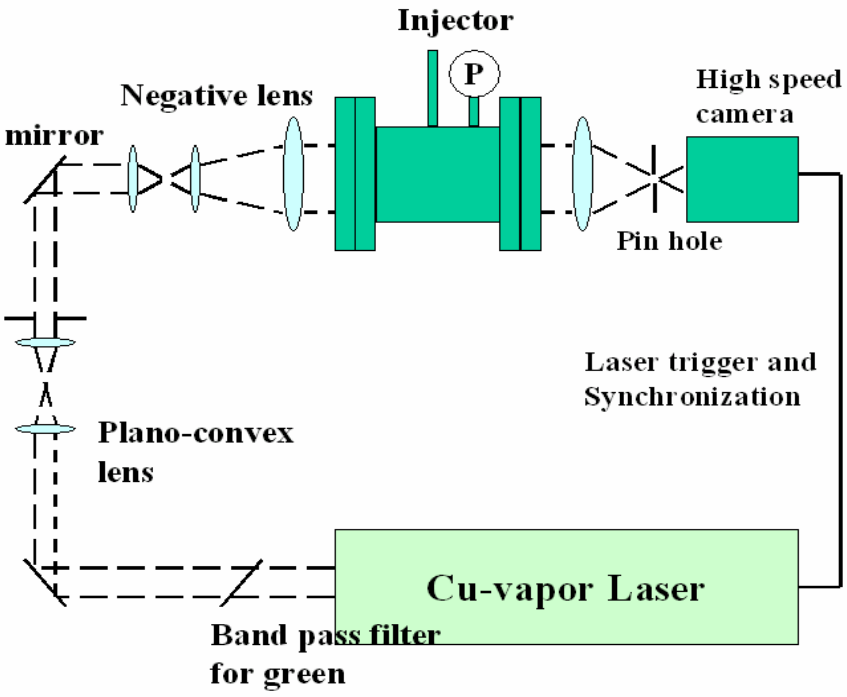

Figure 6 Optical set-up

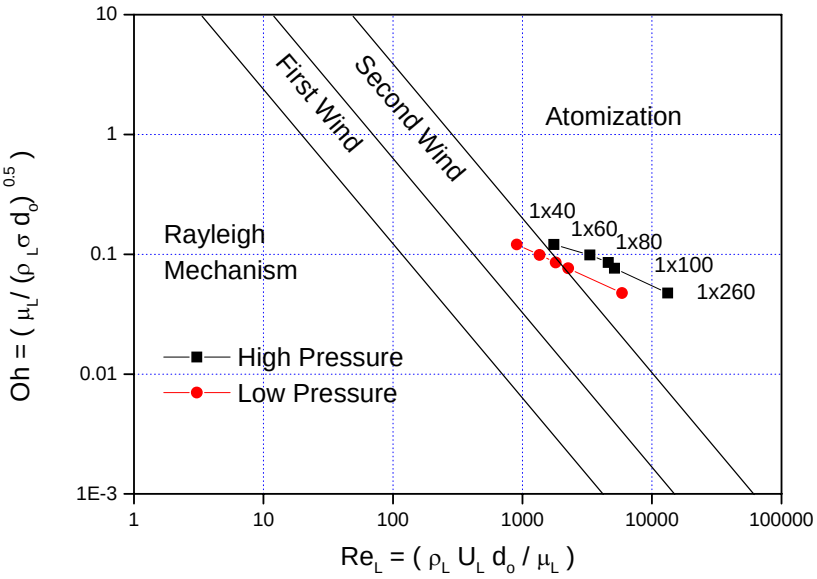

Figure 7 Spray breakup regimes

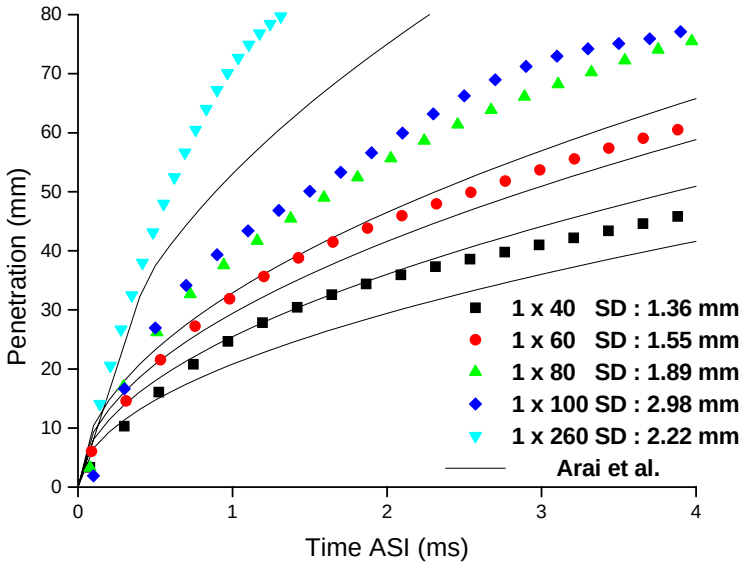

(a)

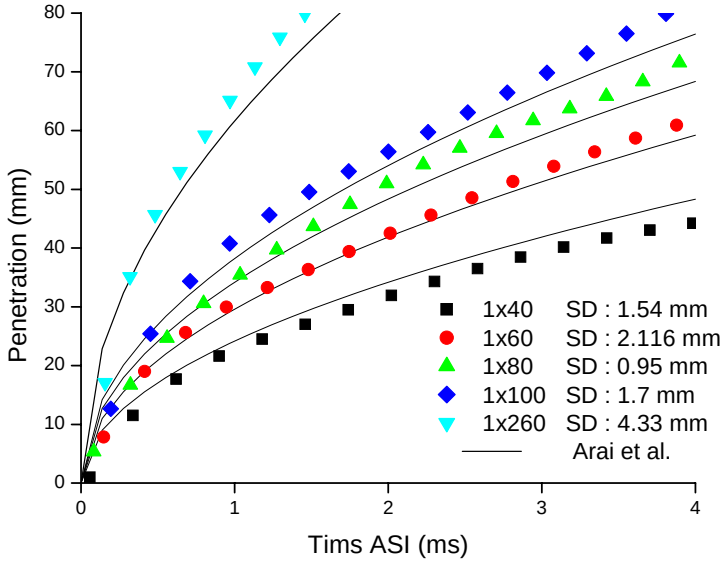

(b)

Figure 8 Polynomial regression curve fits and standard deviations (SD) of spray tip penetration lengths of single orifice nozzles (a) low injection pressures (ρ_{gas}=11.9 kg/m^3) (b) high injection pressures (ρ_{gas}=18.9 kg/m^3)

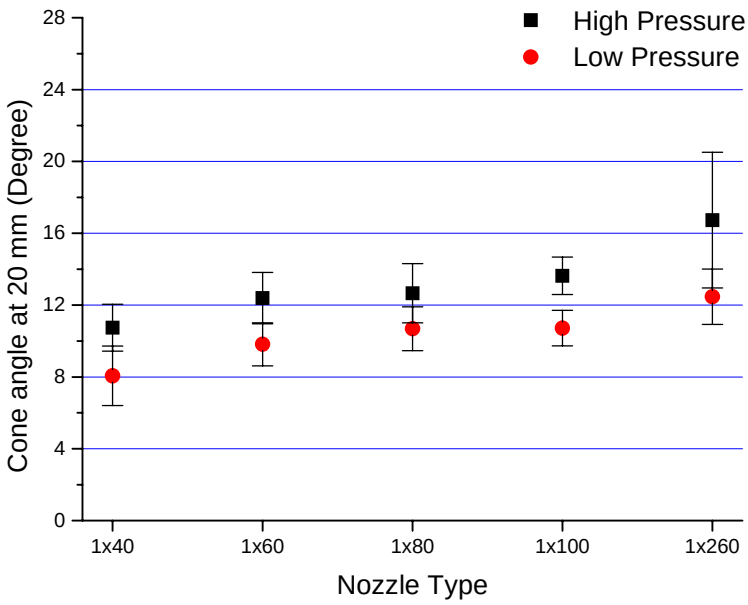

Figure 9 Spray cone angles of single orifice nozzles

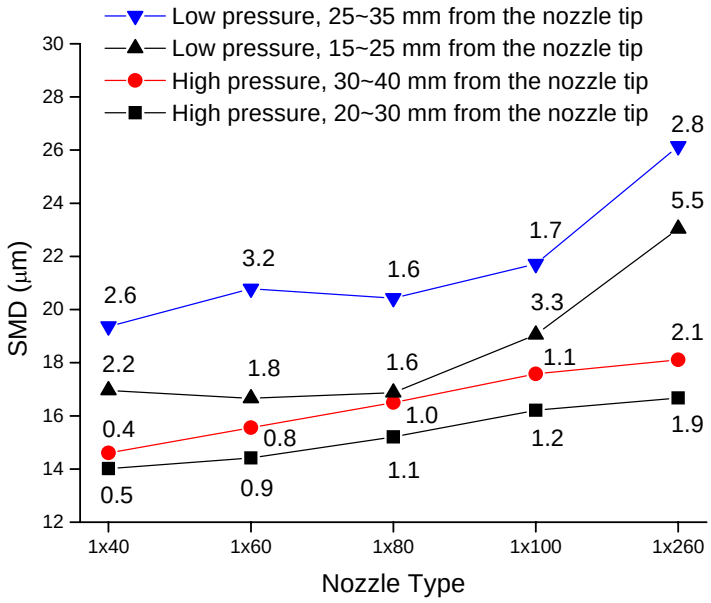

Figure 10 Drop sizes of single orifice nozzles measured using Malvern. Standard deviations in micrometers are shown next to the symbols.

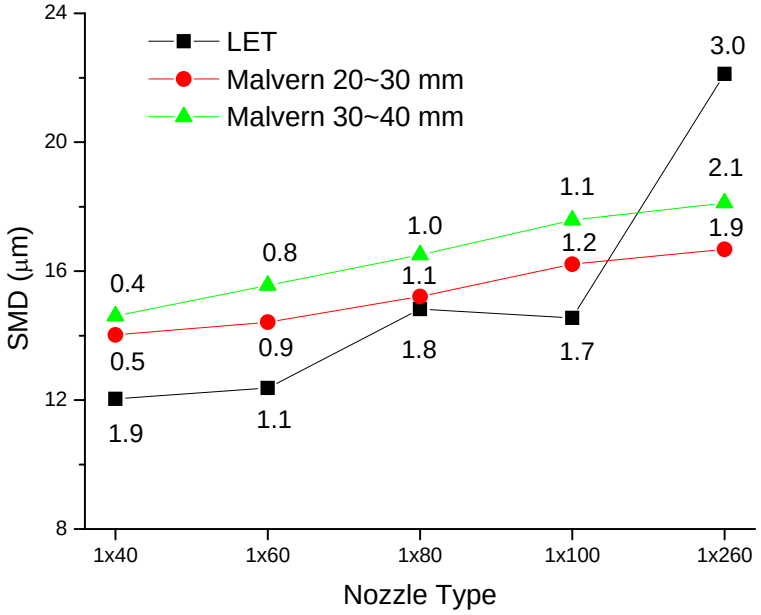

Figure 11 Drop sizes of single orifice nozzles at high injection pressures. Standard deviations in micrometers are shown next to the symbols.

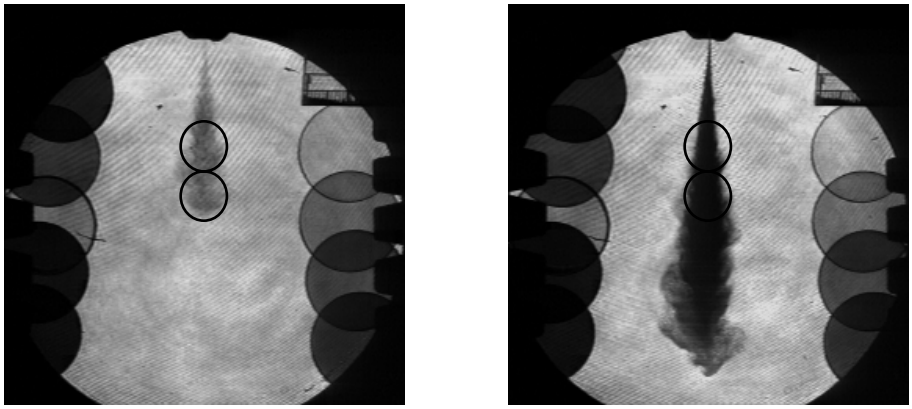

(a) (b)

Figure 12 Spray images at high injection pressures (a) 1x40 at 4 ms after start of injection (b) 1x260 at 1.5 ms after start of injection

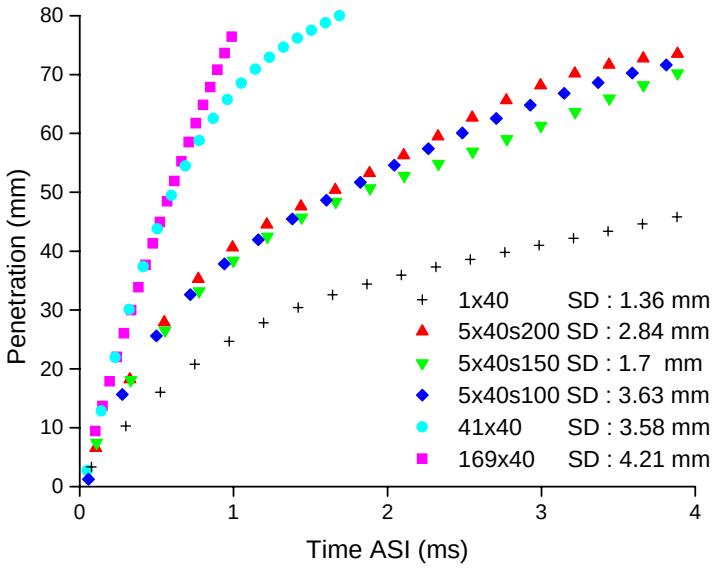

(a)

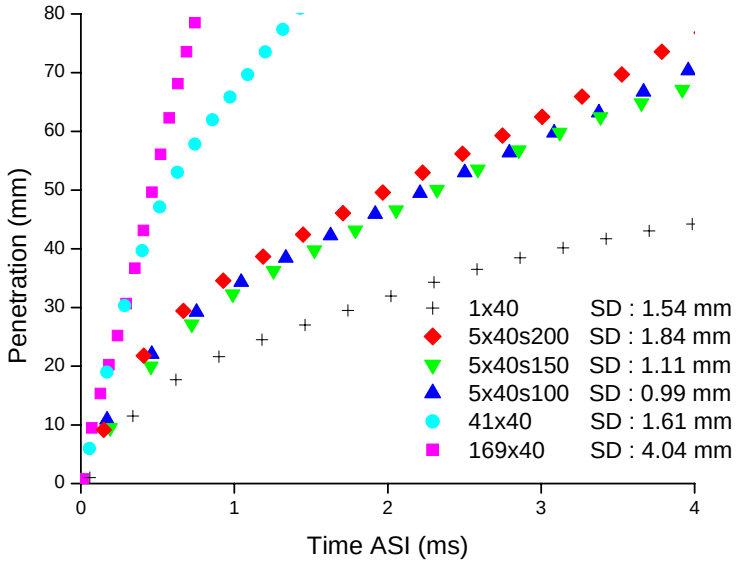

(b)

Figure 13 Polynomial regression curve fits and standard deviations (SD) of spray tip penetration lengths of multiple orifice nozzles (a) low injection pressures (ρ_{gas}=11.9 kg/m^3) (b) high injection pressures (ρ_{gas}=18.9 kg/m^3)

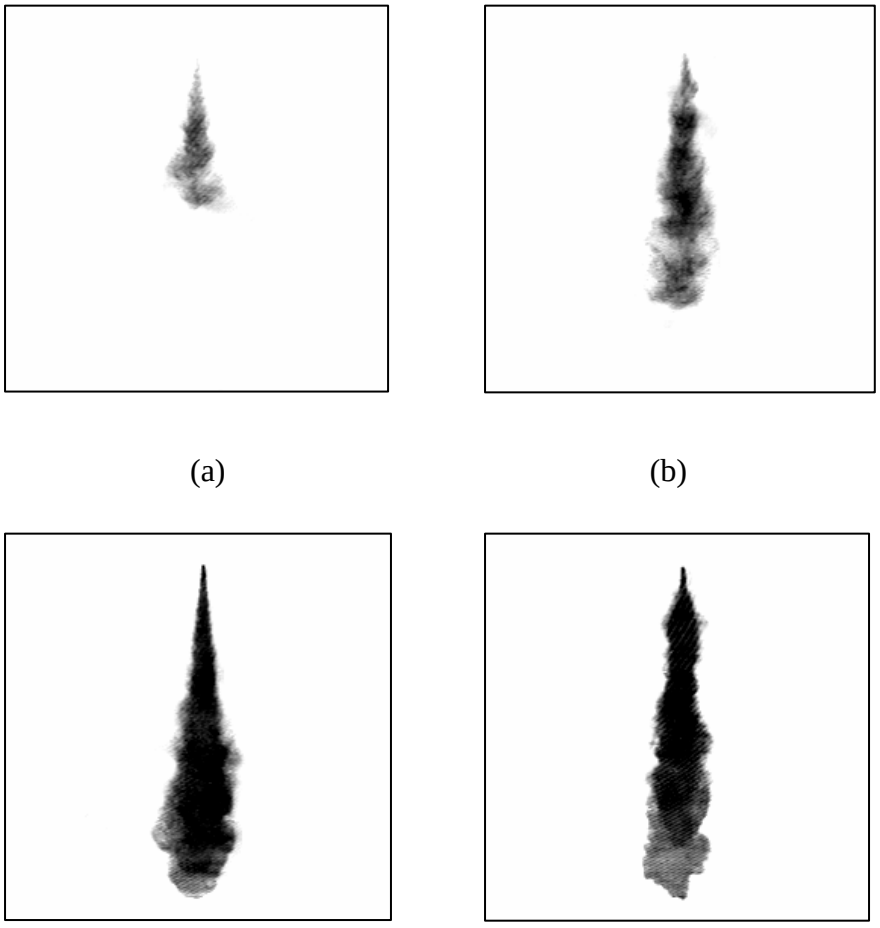

Figure 14 Spray images at high injection pressures (a) 1x40 at 4 ms after start of injection (b) 5x40s200 at 4 ms after start of injection (c) 41x40 at 1.5 ms after start of injection (d) 169x40 at 0.7 ms after start of injection

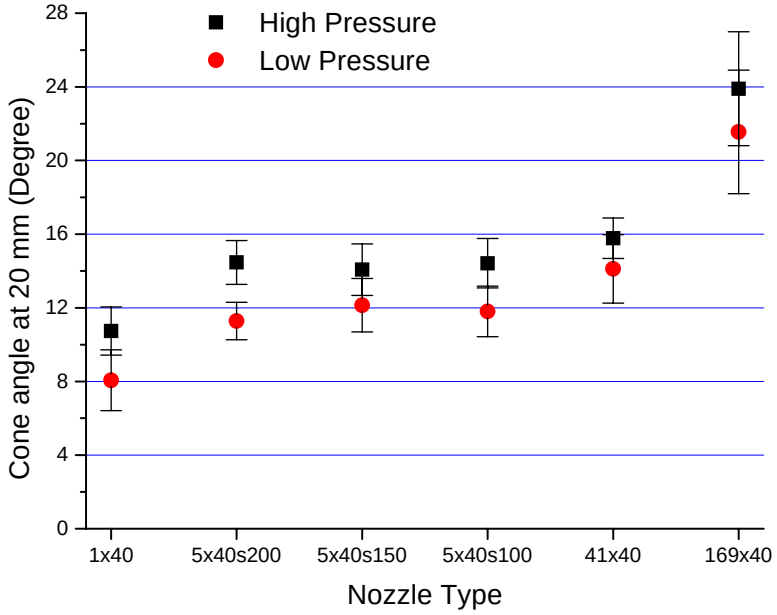

Figure 15 Spray cone angles of multiple orifice nozzles

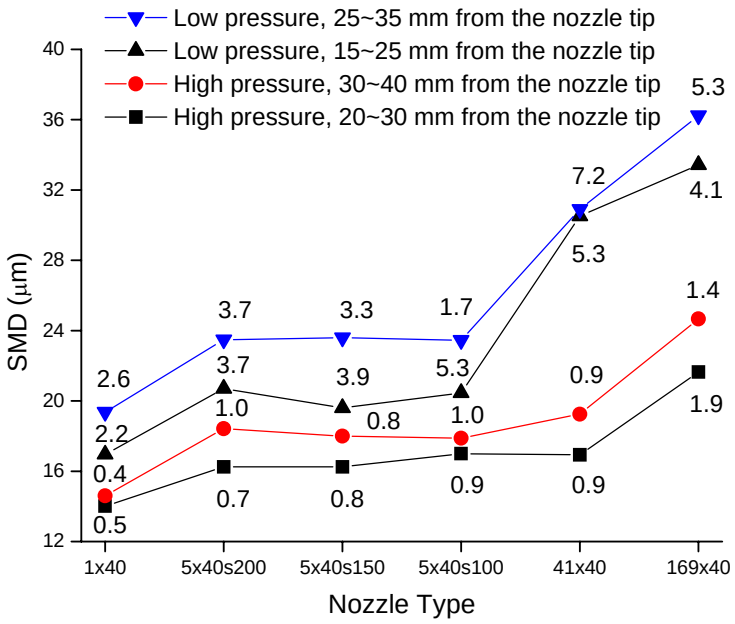

Figure 16 Drop sizes of multiple orifice nozzles measured using Malvern. Standard deviations in micrometers are shown next to the symbols.

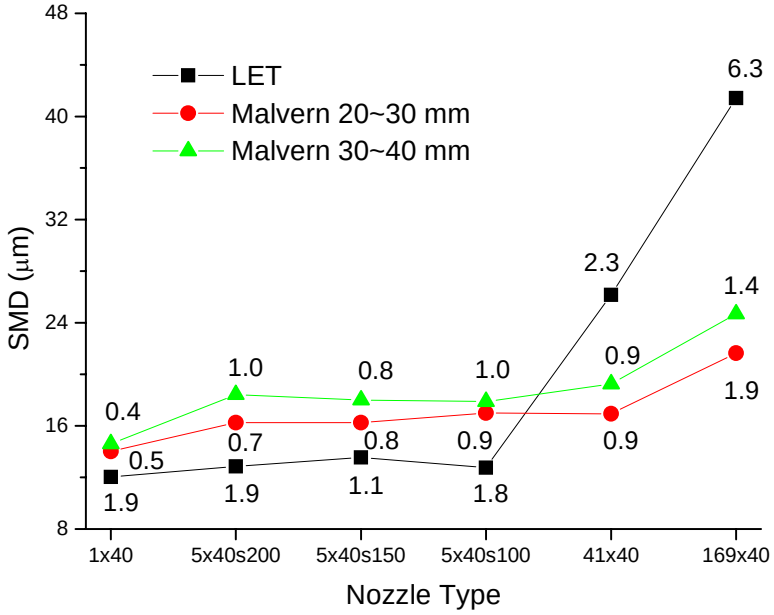

Figure 17 Drop sizes of multiple orifice nozzles at high injection pressures. Standard deviations in micrometers are shown next to the symbols.

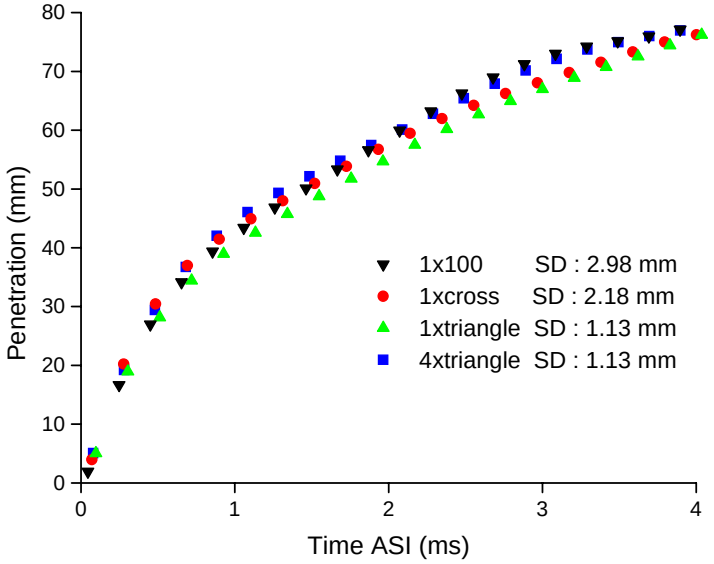

(a)

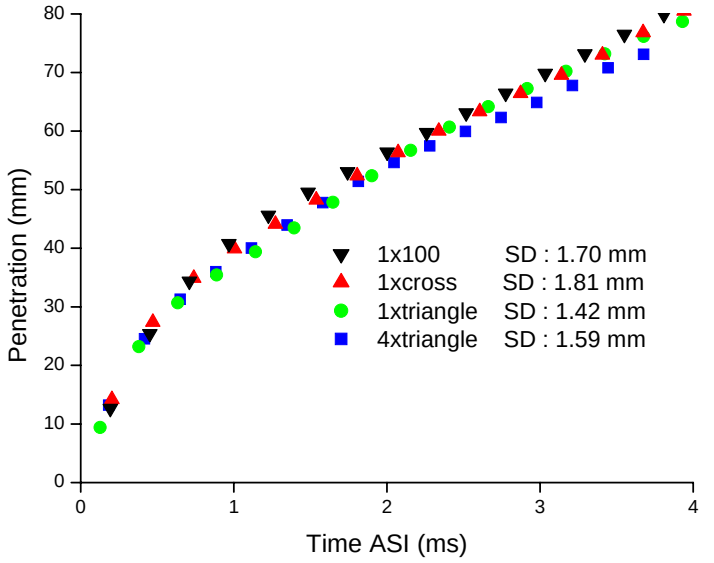

(b)

Figure 18 Polynomial regression curve fits and standard deviations (SD) of spray tip penetration lengths of different orifice shape nozzles (a) low injection pressures (ρ_{gas}=11.9 kg/m^3) (b) high injection pressures (ρ_{gas}=18.9 kg/m^3)

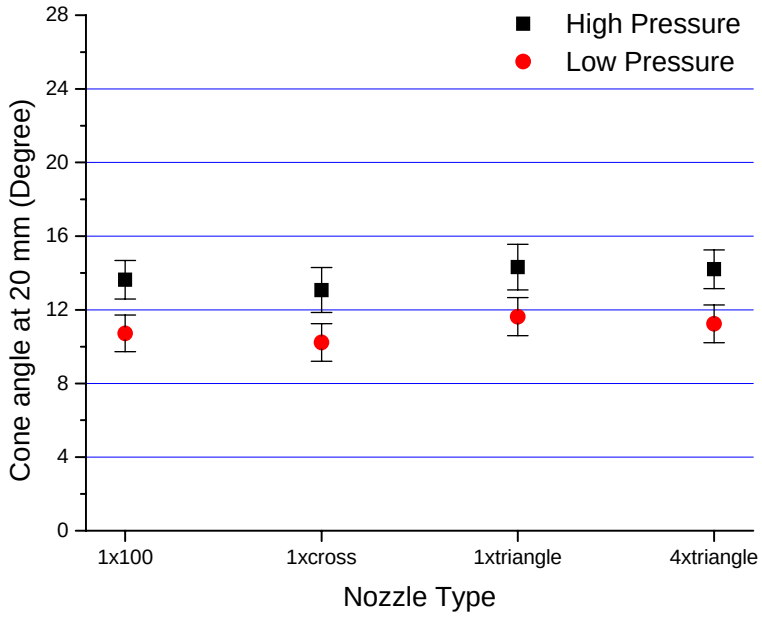

Figure 19 Spray cone angles of different orifice shape nozzles

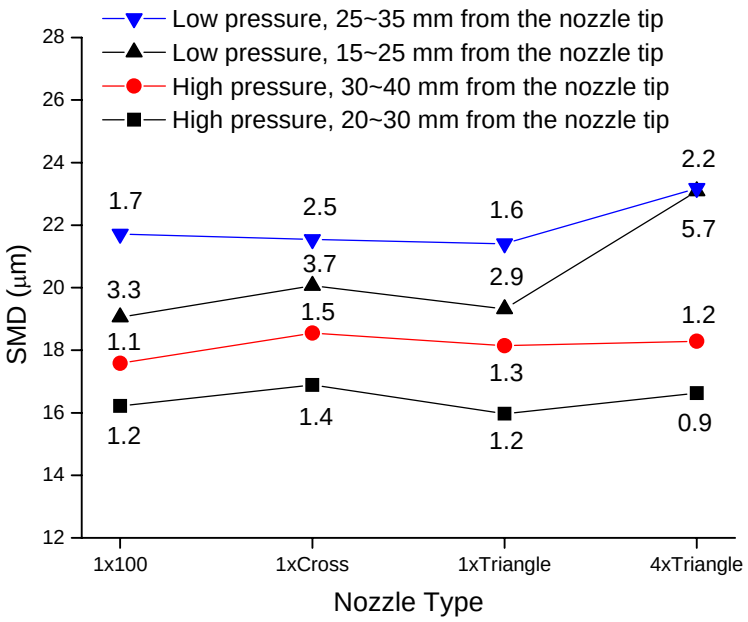

Figure 20 Drop sizes of different orifice shape nozzles measured using Malvern. Standard deviations in micrometers are shown next to the symbols.

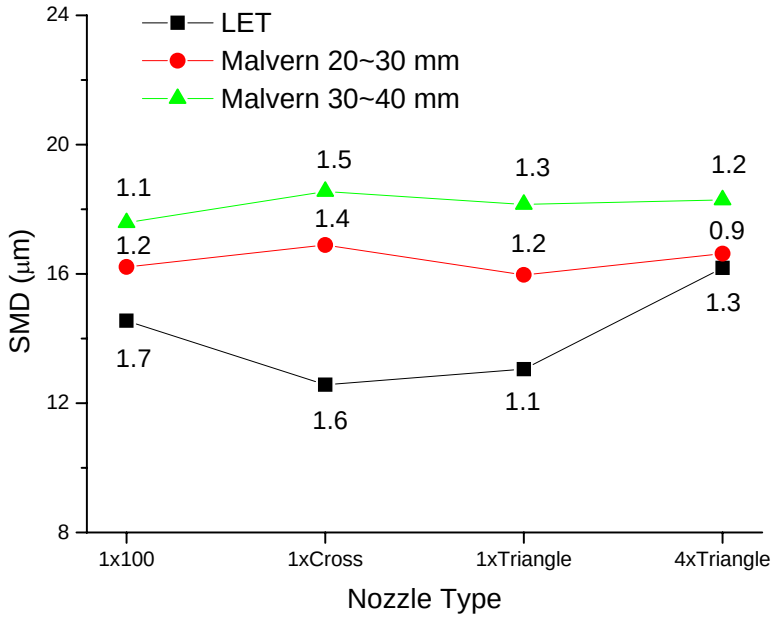

Figure 21 Drop sizes of different orifice shape nozzles at high injection pressures. Standard deviations in micrometers are shown next to the symbols.

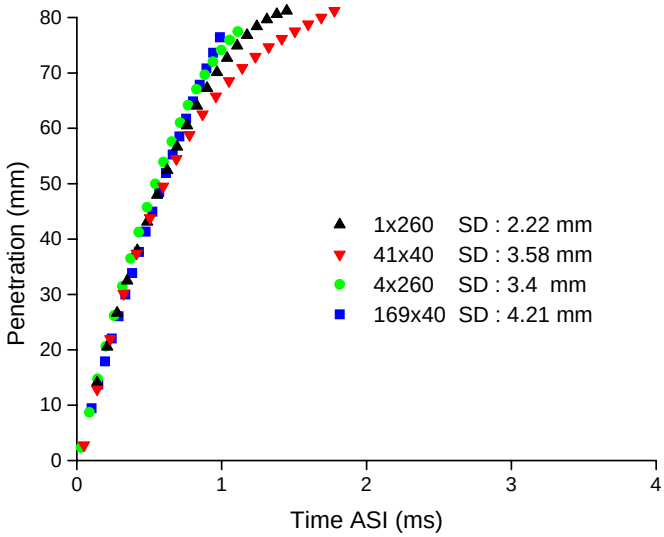

(a)

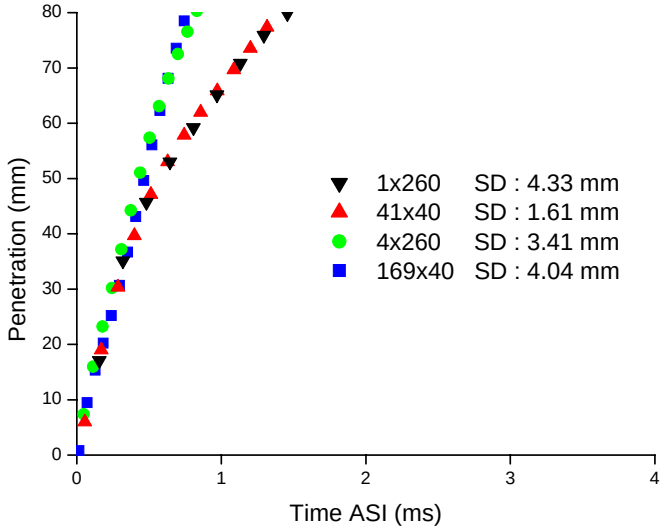

(b)

Figure 22 Polynomial regression curve fits and standard deviations (SD) of spray tip penetration lengths of shower head nozzles (a) low injection pressures (ρ_{gas}=11.9 kg/m^3) (b) high injection pressures (ρ_{gas}=18.9 kg/m^3)

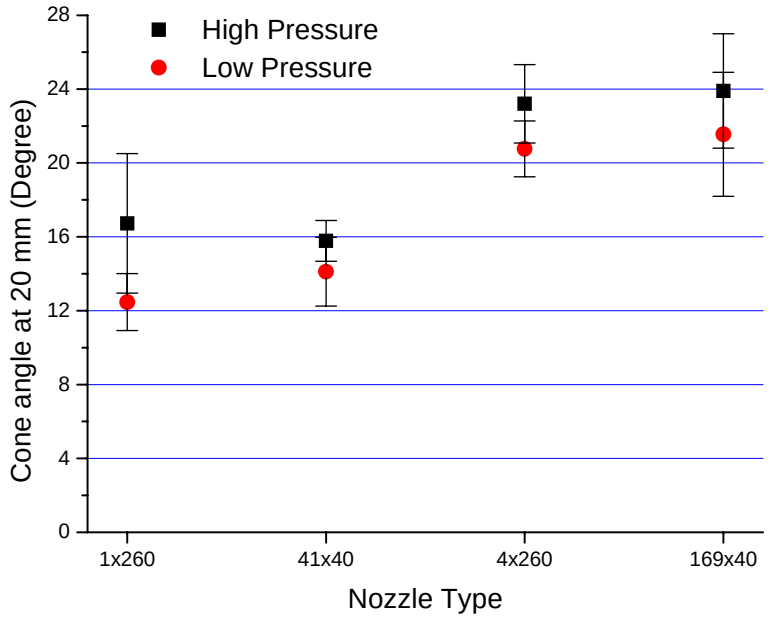

Figure 23 Spray cone angles of shower head nozzles

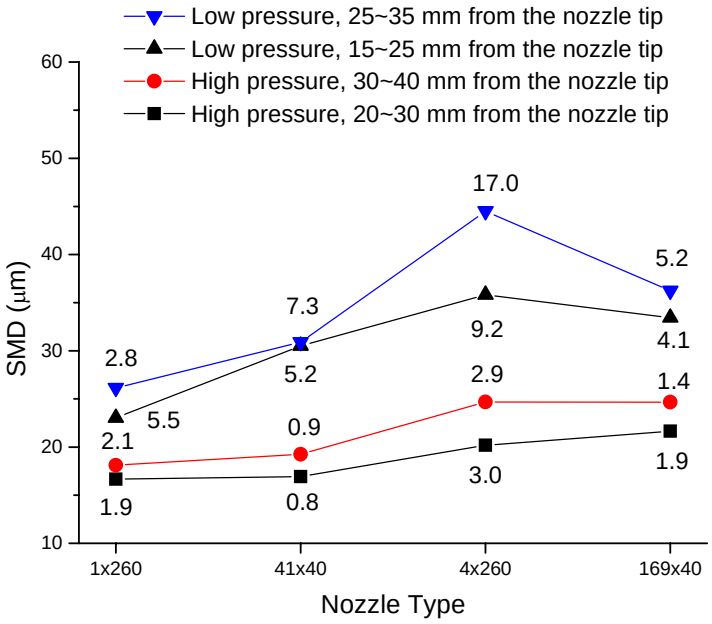

Figure 24 Drop sizes of shower head nozzles measured using Malvern. Standard deviations in micrometers are shown next to the symbols.

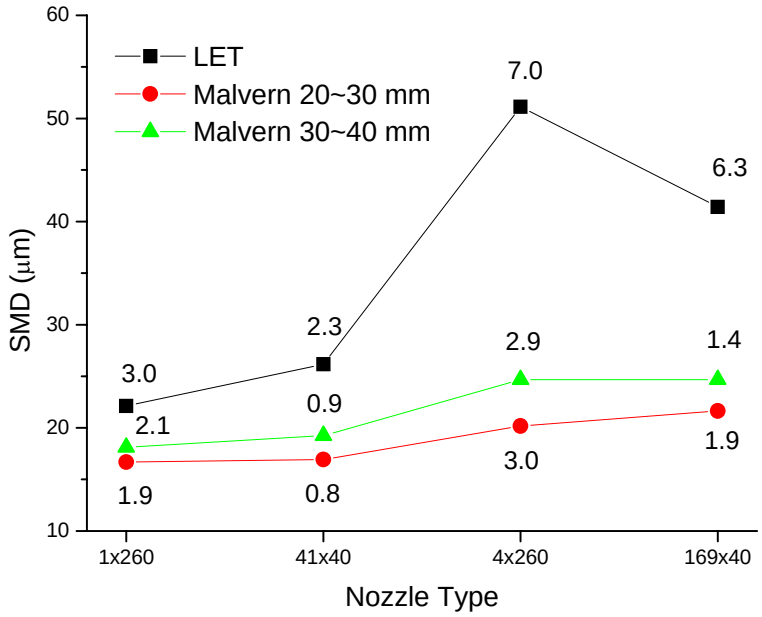

Figure 25 Drop sizes of shower head nozzles at high injection pressures. Standard deviations in micrometers are shown next to the symbols.

Single orifice nozzle Multiple orifice nozzle

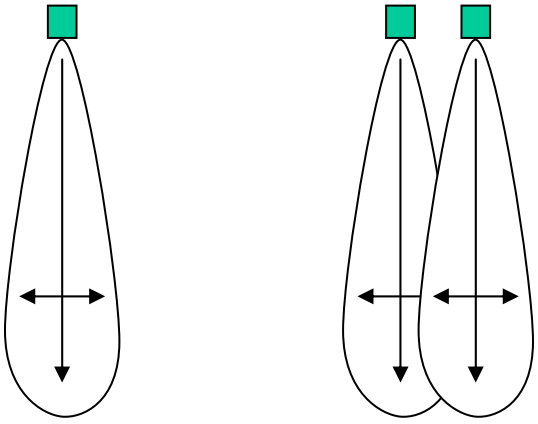

Figure 26 Schematic diagrams of sprays from a single orifice nozzle and a multiple orifice nozzle

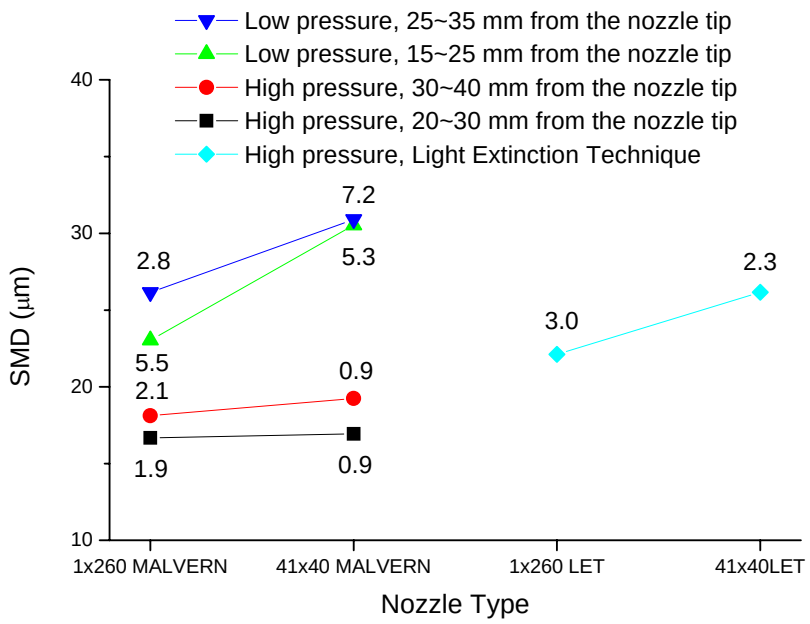

Figure 27 Drop sizes of 1x260 and 41x40. Standard deviations in micrometers are shown next to the symbols.

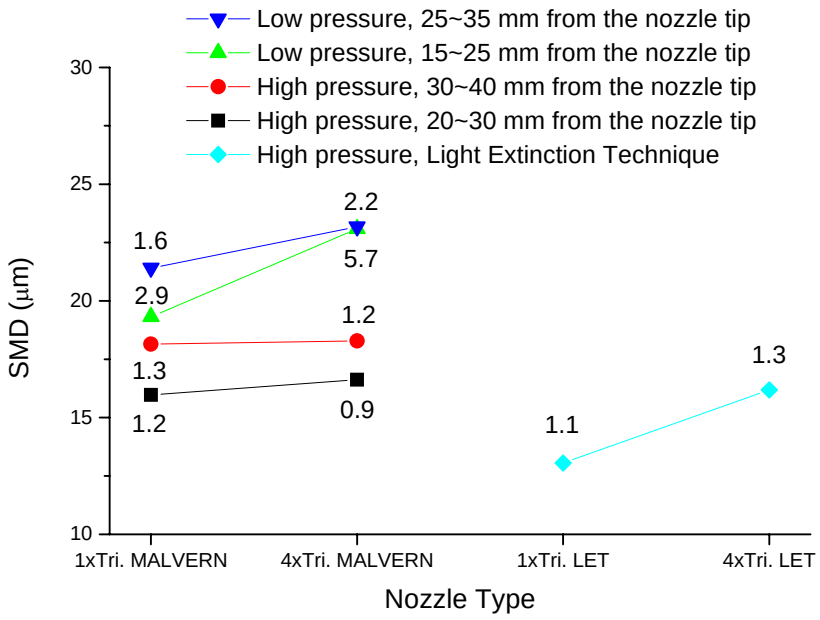

Figure 28 Drop sizes of 1xTriangle and 4xTriangle. Standard deviations in micrometers are shown next to the symbols.

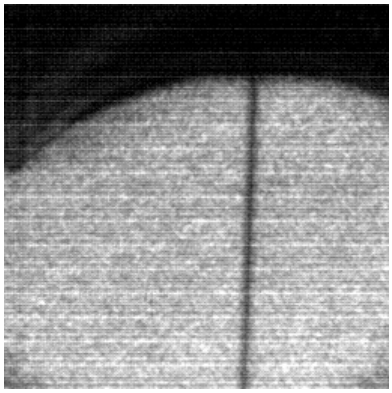

(a)

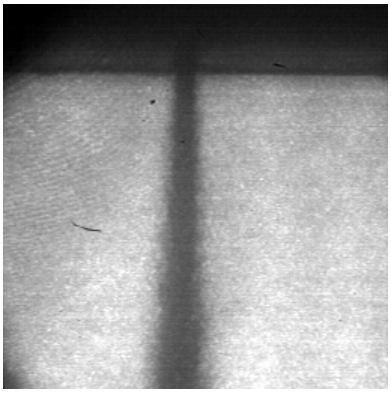

(b)

Figure 29 Spray images of 1x40 (a) low injection pressure image at 2.2 ms after start of injection (b) high injection pressure image at 2.2 ms after start of injection

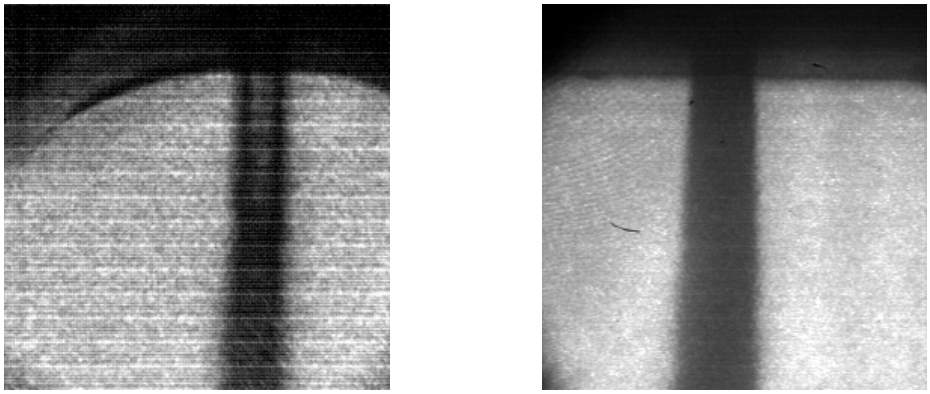

(a) (b)

Figure 30 Spray images of 1x260 (a) low injection pressure image at 2.2 ms after start of injection (b) high injection pressure image at 2.2 ms after start of injection

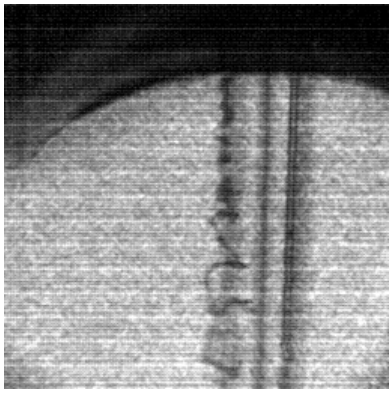

(a)

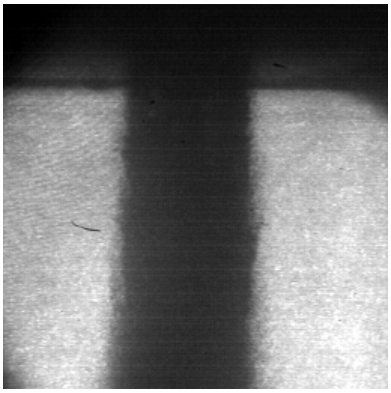

(b)

Figure 31 Spray images of 5x40s200 (a) low injection pressure image at 2.2 ms after start of injection (b) high injection pressure image at 2.2 ms after start of injection

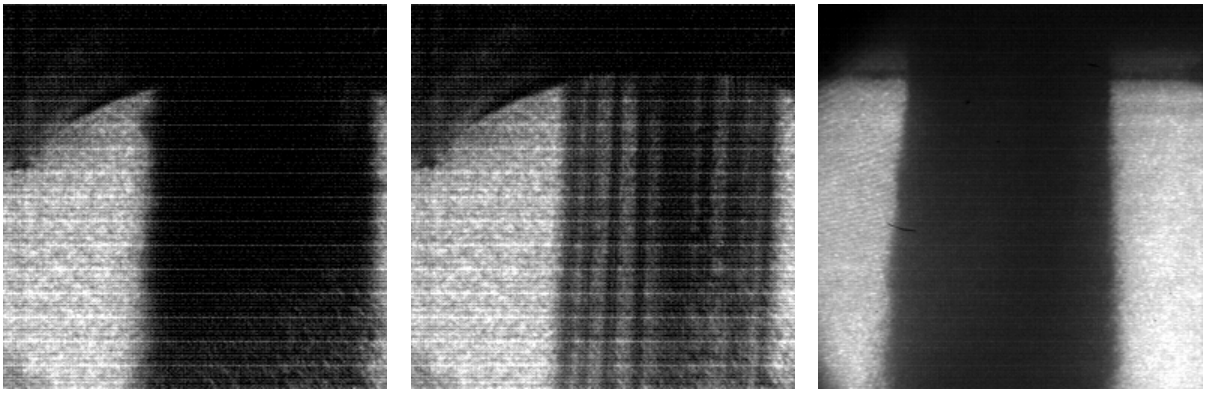

(a) (b) (c)

Figure 32 Spray images of 41x40 (a) low injection pressure image at 2.2 ms after start of injection (b) low injection pressure image at 4.4 ms after start of injection (same injection) (c) high injection pressure image at 2.2 ms after start of injection

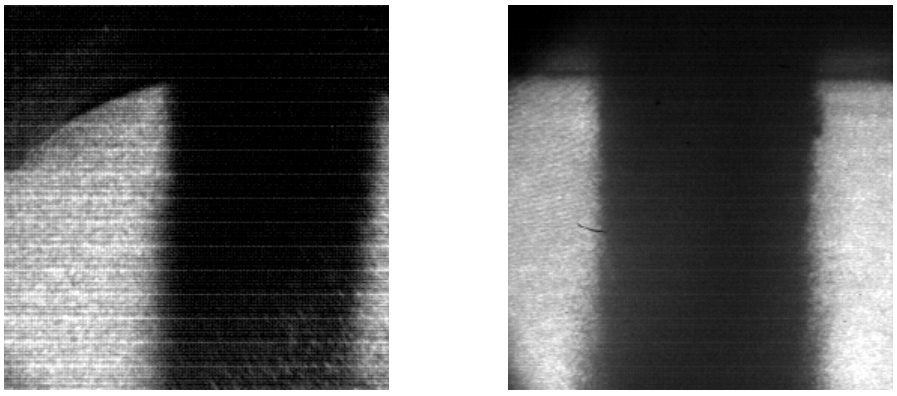

(a) (b)

Figure 33 Spray images of 169x40 (a) low injection pressure image at 2.2 ms after start of injection (b) high injection pressure image at 2.2 ms after start of injection

List of Tables

Table 1. Micro-planar orifice nozzles

Table 2. Experimental conditions

Figure Captions

Figure 1 Micro-planar orifice nozzles - I (a) 1x40 (b) 4x260 (c) 5x40s150 (d) 41x40

Figure 2 Micro-planar orifice nozzles - II (a) 169x40 (b) 1xCross (c) 1xTriangle (d) 4xTriangle

Figure 3 The mechanical retainer design

Figure 4 Injection pressure sensor locations

Figure 5 Injection pressure profiles (a) low injection pressures (b) high injection pressures

Figure 6 Optical set-up

Figure 7 Spray breakup regimes

Figure 8 Polynomial regression curve fits and standard deviations (SD) of spray tip penetration lengths of single orifice nozzles (a) low injection pressures (ρ_{gas}=11.9 kg/m^3) (b) high injection pressures (ρ_{gas}=18.9 kg/m^3)

Figure 9 Spray cone angles of single orifice nozzles

Figure 10 Drop sizes of single orifice nozzles measured using Malvern. Standard deviations in micrometers are shown next to the symbols.

Figure 11 Drop sizes of single orifice nozzles at high injection pressures. Standard deviations in micrometers are shown next to the symbols.

Figure 12 Spray images at high injection pressures (a) 1x40 at 4 ms after start of injection (b) 1x260 at 1.5 ms after start of injection

Figure 13 Polynomial regression curve fits and standard deviations (SD) of spray tip penetration lengths of multiple orifice nozzles (a) low injection pressures (ρ_{gas}=11.9 kg/m^3) (b) high injection pressures (ρ_{gas}=18.9 kg/m^3)

Figure 14 Spray images at high injection pressures (a) 1x40 at 4 ms after start of injection (b) 5x40s200 at 4 ms after start of injection (c) 41x40 at 1.5 ms after start of injection (d) 169x40 at 0.7 ms after start of injection

Figure 15 Spray cone angles of multiple orifice nozzles

Figure 16 Drop sizes of multiple orifice nozzles measured using Malvern. Standard deviations in micrometers are shown next to the symbols.

Figure 17 Drop sizes of multiple orifice nozzles at high injection pressures. Standard deviations in micrometers are shown next to the symbols.

Figure 18 Polynomial regression curve fits and standard deviations (SD) of spray tip penetration lengths of different orifice shape nozzles (a) low injection pressures (ρ_{gas}=11.9 kg/m^3) (b) high injection pressures (ρ_{gas}=18.9 kg/m^3)

Figure 19 Spray cone angles of different orifice shape nozzles

Figure 20 Drop sizes of different orifice shape nozzles measured using Malvern. Standard deviations in micrometers are shown next to the symbols.

Figure 21 Drop sizes of different orifice shape nozzles at high injection pressures. Standard deviations in micrometers are shown next to the symbols.

Figure 22 Polynomial regression curve fits and standard deviations (SD) of spray tip penetration lengths of shower head nozzles (a) low injection pressures (ρ_{gas}=11.9 kg/m^3) (b) high injection pressures (ρ_{gas}=18.9 kg/m^3)

Figure 23 Spray cone angles of shower head nozzles

Figure 24 Drop sizes of shower head nozzles measured using Malvern. Standard deviations in micrometers are shown next to the symbols.

Figure 25 Drop sizes of shower head nozzles at high injection pressures. Standard deviations in micrometers are shown next to the symbols.

Figure 26 Schematic diagrams of sprays from a single orifice nozzle and a multiple orifice nozzle

Figure 27 Drop sizes of 1x260 and 41x40. Standard deviations in micrometers are shown next to the symbols.

Figure 28 Drop sizes of 1xTriangle and 4xTriangle. Standard deviations in micrometers are shown next to the symbols.

Figure 29 Spray images of 1x40 (a) low injection pressure image at 2.2 ms after start of injection (b) high injection pressure image at 2.2 ms after start of injection

Figure 30 Spray images of 1x260 (a) low injection pressure image at 2.2 ms after start of injection (b) high injection pressure image at 2.2 ms after start of injection

Figure 31 Spray images of 5x40s200 (a) low injection pressure image at 2.2 ms after start of injection (b) high injection pressure image at 2.2 ms after start of injection

Figure 32 Spray images of 41x40 (a) low injection pressure image at 2.2 ms after start of injection (b) low injection pressure image at 4.4 ms after start of injection (same injection) (c) high injection pressure image at 2.2 ms after start of injection

Figure 33 Spray images of 169x40 (a) low injection pressure image at 2.2 ms after start of injection (b) high injection pressure image at 2.2 ms after start of injection